27. T. J. Stasevich, C. G. Tao, W. G. Cullen, E. D. Williams, T. L. Einstein, *Phys. Rev. Lett.* **102**, 085501 (2009).
28. P. J. Rous, *Phys. Rev. B* **59**, 7719 (1999).
29. Y. N. Mo, W. G. Zhu, E. Kaxiras, Z. Y. Zhang, *Phys. Rev. Lett.* **101**, 216101 (2008).
30. J. Y. Park *et al.*, *Phys. Rev. Lett.* **95**, 136802 (2005).
31. A. Sperl *et al.*, *Phys. Rev. B* **77**, 085422 (2008).
32. R. S. Sorbello, *Solid State Phys.* **51**, 159 (1997).
33. J. Taylor, H. Guo, J. Wang, *Phys. Rev. B* **63**, 245407 (2001).
34. B. G. Briner, R. M. Feenstra, T. P. Chin, J. M. Woodall, *Phys. Rev. B* **54**, R5283 (1996).
35. J. Homoth *et al.*, *Nano Lett.* **9**, 1588 (2009).
36. Y. Zhang, W. van Drongelen, B. He, T. Block, C. Tegenkamp, *Appl. Phys. Lett.* **89**, 223903 (2006).
37. C. Jin, K. Suenaga, S. Iijima, *Nano Lett.* **8**, 1127 (2008).
38. T. Sun *et al.*, *Phys. Rev. B* **79**, 041402 (2009).
39. M. Rusanen, P. Kuhn, J. Krug, *Phys. Rev. B* **74**, 245423 (2006).
40. D. Dundas, E. J. McEniry, T. N. Todorov, *Nat. Nanotechnol.* **4**, 99 (2009).
41. This work has been supported by the University of Maryland NSF Materials Research Science and Engineering Center under grant DMR 05-20471, including use of the Shared Experimental Facilities. Infrastructure support is also provided by the University of Maryland NanoCenter and the Center for Nanophysics and Advanced Materials.

Supporting Online Material
www.sciencemag.org/cgi/content/full/328/5979/736/DC1
Materials and Methods
Figs. S1 to S4
References
Movie S1

4 January 2010; accepted 7 April 2010
10.1126/science.1186648

Viscosity of $MgSiO_3$ Liquid at Earth's Mantle Conditions: Implications for an Early Magma Ocean

Bijaya B. Karki[1]* and Lars P. Stixrude[2]

Understanding the chemical and thermal evolution of Earth requires knowledge of transport properties of silicate melts at high pressure and high temperature. Here, first-principles molecular dynamics simulations show that the viscosity of $MgSiO_3$ liquid varies by two orders of magnitude over the mantle pressure regime. Addition of water systematically lowers the viscosity, consistent with enhanced structural depolymerization. The combined effects of pressure and temperature along model geotherms lead to a 10-fold increase in viscosity with depth from the surface to the base of the mantle. Based on these calculations, efficient heat flux from a deep magma ocean may have exceeded the incoming solar flux early in Earth's history.

Silicate liquids likely played a crucial role in terrestrial mass and heat transport in Earth's history. Molten silicates would have controlled the dynamics of the predicted magma ocean [a largely or completely molten mantle that is expected during Earth's earliest stages (*1*)] and continue to influence the transport of modern magmas at the present. If such a magma ocean existed, the rates of initial thermal evolution (via convection) and chemical evolution (via crystal settling and melt percolation) of Earth's interior would be primarily controlled by the melt viscosity (*2*). The ability of melts to carry xenoliths from great depths in the mantle (*3*) also depends on the melt viscosity, in addition to melt composition. Moreover, melts are considered to be responsible for the ultralow velocity zone (ULVZ) in the deep mantle detected by seismology (*4*, *5*).

Despite their importance, transport properties, including the viscosity of molten silicates, are unknown over almost the entire mantle pressure regime, which reaches 136 GPa at the core-mantle boundary. Because of experimental difficulties, the viscosity of $MgSiO_3$ liquid, the dominant composition of Earth's mantle, has only been measured at ambient pressures (*6*). In fact, viscosity measurements of any silicate melts have been limited to relatively low pressures (<13 GPa) (*7*–*12*). In many silicate liquids, the viscosity depends non-monotonically on pressure over the range that has been measured, making extrapolations highly uncertain. Theoretical computations serve as a complementary approach. Previous calculations were primarily based on atomistic models (*13*–*15*), which permit much faster computation but have the disadvantage of being based on empirical force fields, the forms of which are uncertain. On the other hand, the first-principles approach is more robust because it makes no assumptions about the nature of bonding or the shape of the charge density and is thus in principle equally applicable to the study of a wide variety of materials problems, including liquids. We previously calculated the structure and thermodynamic properties of $MgSiO_3$ and $MgSiO_3$-H_2O liquids from first principles (*16*, *17*), finding good agreement with extant experimental data over the entire mantle pressure-temperature regime. Unlike these equilibrium properties, the transport properties such as viscosity require much longer simulation (*18*).

Here, we determine the viscosity of two key liquids over the entire mantle pressure regime from density functional theory (*18*). $MgSiO_3$ serves as an analog composition for a magma ocean, whereas $MgSiO_3$-H_2O liquid allows us to explore the role of melt composition, focusing on H_2O as the component that is known to have the largest influence on the viscosity at low pressure (*19*). The shear viscosity (η) was calculated by using the Green-Kubo relation

$$\eta = \frac{V}{3k_B T}\int_0 \left\langle \sum_{i<j} \sigma_{ij}(t+t_0).\sigma_{ij}(t_0) \right\rangle dt \quad (1)$$

where σ_{ij} (i and $j = x, y, z$) is the stress tensor, which is computed directly at every time step of the simulation, V is volume, k_B is the Boltzmann constant, T is temperature, t is time, and t_0 represents the time origin. The shear-stress autocorrelation function (the integrand of Eq. 1) decays to zero more slowly at lower temperature and higher pressure, requiring longer simulation

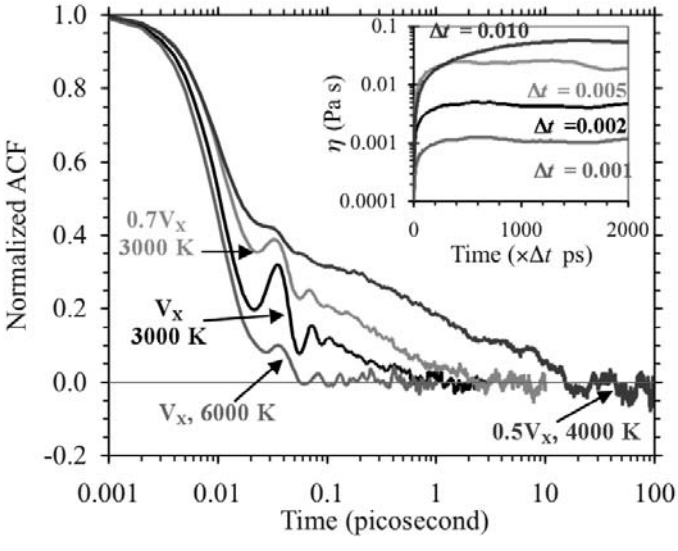

Fig. 1. Time convergences of the calculated stress autocorrelation function (ACF) and viscosity (**inset**) of $MgSiO_3$ melt (without water) at different conditions. The run durations are 18 ps (V_X, 6000 K, 7.5 GPa), 60 ps (V_X, 3000 K, 1.8 GPa), 72 ps ($0.7V_X$, 3000 K, 25 GPa), and 172 ps ($0.5V_X$, 4000 K, 135 GPa), where V_X is the reference volume (38.9 cm^3mol^{-1}).

[1]Department of Computer Science, Department of Geology and Geophysics, Louisiana State University, Baton Rouge, LA 70803, USA. [2]Department of Earth Sciences, University College London, London WC1E 6BT, UK.

*To whom correspondence should be addressed. E-mail: karki@csc.lsu.edu

runs (Fig. 1). We find that the integral values, and hence the computed viscosity, converge over time intervals much shorter than the total simulation durations (Fig. 1, inset). The fact that the shear stress autocorrelation function decays to zero within the time scale of our simulations means that the Maxwell relaxation time of silicate liquids (*20*) remains much shorter than seismic periods over the entire mantle regime and that seismic wave propagation through melts that may exist in the ULVZ will occur in the relaxed limit. We further confirm that the simulated system is in the liquid state at each pressure-temperature condition by examining the mean-square displacements (fig. S1) and radial distribution functions (fig. S2). Our approach is expected to be more robust than the commonly used indirect approach of estimating the melt viscosity from the self-diffusion coefficient via the classic Erying relation (*20*, *21*). The validity of the Eyring relation as applied to silicate liquids has been questioned on the basis of experiments (*11*).

Over most of the pressure range of our investigation, viscosity increases with increasing pressure (Fig. 2A). The calculated viscosity increases by a factor of ~140 for anhydrous silicate melt over the entire mantle pressure regime at 4000 K. The activation volume $V_\eta^* = (d\ln\eta/dP)_T$ varies systematically over most of this range, tending to decrease with increasing pressure and with increasing temperature. At the lowest temperature and pressure, we find that the viscosity behaves anomalously: decreasing with increasing pressure initially, reaching a minimum value near 5 GPa at 3000 K, and then increasing on further compression. Low-pressure experimental studies have found viscosity decreasing with increasing pressure in highly polymerized silicate melts (*8*, *11*, *23*). We attribute the initial decrease in viscosity with increasing pressure to the presence of fivefold coordinated silicon, which acts as a transition state accommodating viscous flow (*16*, *24*). The variation of viscosity in this anomalous regime is small compared with the total variation in viscosity over the mantle pressure-temperature range. The calculated viscosities show large and systematic deviations from Arrhenian behavior (Fig. 2B). The activation energy decreases with increasing temperature, consistent with the behavior of moderately fragile liquids (*25*).

Silicate melt with 10 weight percent H_2O is two to four times less viscous than the anhydrous melt at all pressure-temperature conditions studied (Fig. 2). We have previously shown that the self-diffusion coefficients of the hydrous liquid are systematically higher than those of the anhydrous liquid (*26*). The region of anomalous pressure dependence of the viscosity and diffusion are weak or absent in the case of hydrous silicate liquid. Our first-principles results confirm that the dynamical enhancement (smaller viscosity and larger diffusivity) occurs in hydrous silicate liquid because water systematically depolymerizes the melt structure (*27*). The mean O-Si and Si-Si coordination numbers decrease in the presence of water: The hydrous values vary from 1.1 to 1.7 on compression (compared with anhydrous value of 1.4 to 2) and 1.8 to 4.7 (compared with anhydrous value of 2.5 to 5.5), respectively, over the compression range studied (*17*, *26*).

The viscosity of silicate melts increases modestly along temperature profiles characteristic of Earth's interior because of the competing effects of pressure and temperature (Fig. 3). For example, along a slightly super-liquidus magma ocean isentrope (*28*), the viscosity of anhydrous melt increases by a factor of 10 from the surface to the core-mantle boundary. The variations are similar in size but non-monotonic along the estimated mantle solidus and liquidus (*28*). The non-monotonic variation of the viscosity along these curves is due to the rapid increase in temperature with increasing pressure at low pressure. The viscosity profiles of the hydrous melt show similar variations but are systematically shifted downward (Fig. 3).

Our results provide a fundamental basis for any dynamical model of magma ocean evolution. To illustrate, we use our viscosity results and those of previous ab initio simulations of silicate melts to estimate critical dynamical parameters. For a completely molten mantle such as one that may have occurred early in Earth's history (*1*), the estimated Rayleigh and Prandtl numbers (*29*) are ~6×10^{30} and ~60, respectively, for the viscosity value of 0.048(10) Pa s for anhydrous $MgSiO_3$ liquid at mid-mantle condition (70 GPa

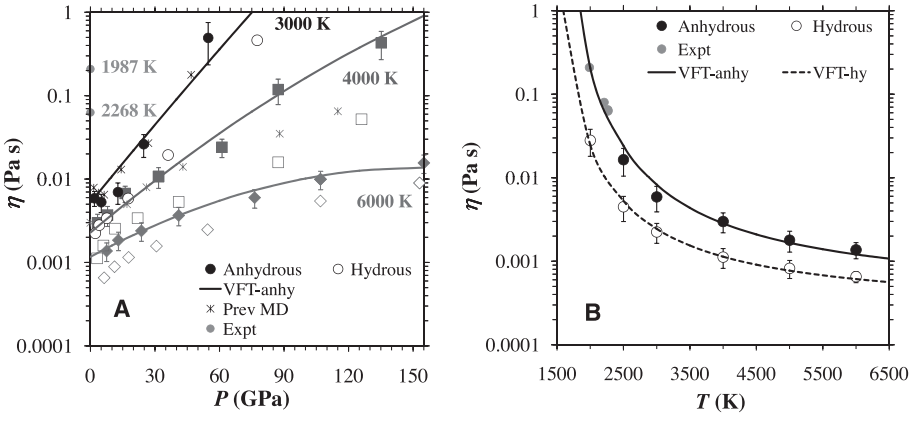

Fig. 2. Calculated viscosity (η) of anhydrous (anhy, solid symbols) and hydrous (hy, open symbols) $MgSiO_3$ melts. Our results are compared with experimental (Expt) data (*6*) at lower temperatures and ambient pressure for anhydrous $MgSiO_3$ liquid. Error bars indicate the statistical uncertainties. (**A**) Pressure variations along 3000 K (circles), 4000 K (squares), and 6000 K (diamonds) isotherms. The anhydrous results can be represented by the modified VFT (Vogel-Fulcher-Tammann) equation (*35*): $\eta(P,T) = \exp[-7.75 + 0.005\,P - 0.00015\,P^2 + (5000 + 135\,P + 0.23P^2)/(T - T_0)]$, with T_0 = 1000 K. Also shown are the results at 3000 K (*14*) and 4000 K (*15*) from previous molecular dynamics (MD) studies of anhydrous liquid based on semi-empirical pair potentials. (**B**) Temperature variations at the reference volume (V_X) together with experimental data (*6*) represented by the VFT equation, $\eta(T) = A\,\exp[\,B/(T - 1000)]$, where A = 0.00033 Pa s and B = 6400 K for anhydrous liquid and A = 0.00024 Pa s and B = 4600 K for hydrous liquid.

Fig. 3. Predicted viscosity for magma ocean based on anhydrous silicate liquid results (using the modified VFT relation shown in Fig. 2) along different temperature profiles (**inset**) from (*28*): magma ocean isentrope, mantle liquidus, mantle solidus, and melting curve of pure $MgSiO_3$ perovskite (dashed line). The hydrous result is shown only along the mantle liquidus (gray line). The symbol represents a viscosity value at mid-mantle condition.

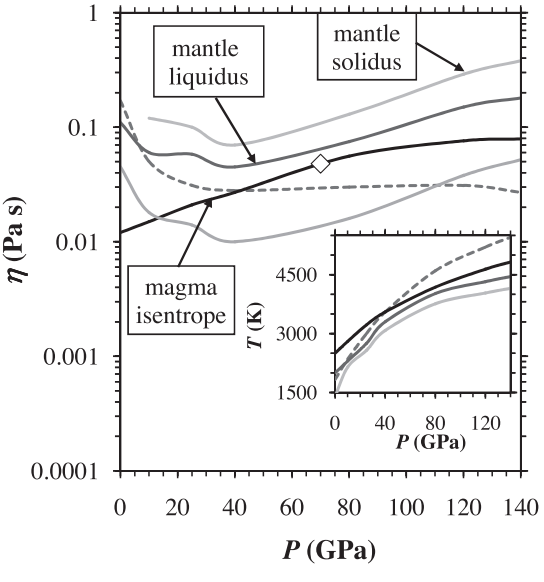

and 4000 K along the magma ocean isentrope, Fig. 3). The Rayleigh number lies in the regime of turbulent convection: The presence of turbulence may substantially influence the settling of crystals as they form upon cooling. The surface heat flux, $F \sim 6 \times 10^4$ W m^{-2}, estimated from mixing length theory far exceeds the incoming solar flux (*30*) and suggests that the surface temperature was set by heat exchange of the magma ocean with a dense silicate atmosphere rather than by solar radiation balance (*2*). This value of F implies a cooling time for the magma ocean ~20 ky (*30*). In fact, a number of processes are likely to increase the cooling time of the magma ocean substantially, including crystallization, which is predicted to initiate in the mid-mantle (*28*) and to separate the magma ocean into upper and basal layers (*31*). The evolution at this stage also depends strongly on the viscosity, which will set the time scale for buoyancy-driven motion of crystals and liquid that can lead to chemical differentiation. The direction of motion will be set by the crystal-liquid density contrast, the sign of which varies with pressure and temperature. Indeed, crystals are expected to float near the base of the mantle (*16*), producing a buoyantly stable basal magma layer that may be long-lived (*31*).

References and Notes

1. R. M. Canup, *Icarus* **168**, 433 (2004).
2. V. S. Solomatov, in *Evolution of the Earth*, D. Stevenson, Ed., vol. 9 of *Treatise on Geophysics*, G. Schubert, Ed. (Elsevier, Amsterdam, 2007), p. 91.
3. S. E. Haggerty, V. Sautter, *Science* **248**, 993 (1990).
4. J. Revenaugh, S. A. Sipkin, *Nature* **369**, 474 (1994).
5. Q. Williams, E. J. Garnero, *Science* **273**, 1528 (1996).
6. G. Urbain, Y. Bottinga, P. Richet, *Geochim. Cosmochim. Acta* **46**, 1061 (1982).
7. I. Kushiro, H. S. Yoder Jr., B. O. Mysen, *J. Geophys. Res.* **81**, 6351 (1976).
8. Y. Bottinga, P. Richet, *Geochim. Cosmochim. Acta* **59**, 2725 (1995).
9. J. E. Reid *et al.*, *Phys. Earth Planet. Inter.* **139**, 45 (2003).
10. H. Behrens, F. Schulze, *Am. Mineral.* **88**, 1351 (2003).
11. D. Tinker *et al.*, *Am. Mineral.* **89**, 1701 (2004).
12. C. Liebske *et al.*, *Earth Planet. Sci. Lett.* **240**, 589 (2005).
13. E. A. Wasserman, D. A. Yuen, J. R. Rustad, *Earth Planet. Sci. Lett.* **114**, 373 (1993).
14. D. J. Lacks, D. Rear, J. A. Van Orman, *Geochim. Cosmochim. Acta* **71**, 1312 (2007).
15. D. Nevins, F. J. Spera, M. S. Ghiorso, *Am. Mineral.* **94**, 975 (2009).
16. L. Stixrude, B. B. Karki, *Science* **310**, 297 (2005).
17. M. Mookherjee, L. Stixrude, B. B. Karki, *Nature* **452**, 983 (2008).
18. Computations were performed by using the VASP software (*32*) with the local density approximation and ultrasoft pseudopotentials as before (*16*, *17*, *26*). Methods are available as supporting material on *Science* Online.
19. L. A. Lange, *Rev. Mineral.* **30**, 331 (1994).
20. M. L. Rivers, I. S. E. Carmichael, *J. Geophys. Res.* **92**, (B9), 9247 (1987).
21. J. Mungall, *Geochim. Cosmochim. Acta* **66**, 125 (2002).
22. T. K. Wan, T. S. Duffy, S. Scandolo, R. Car, *J. Geophys. Res.* **112** (B3), 03208 (2007).
23. G. Giordano, D. B. Dingwell, *Earth Planet. Sci. Lett.* **208**, 337 (2003).
24. C. A. Angell, P. A. Cheeseman, S. Tamaddon, *Science* **218**, 885 (1982).
25. C. A. Angell, *Science* **267**, 1924 (1995).
26. B. B. Karki, D. Bhattarai, M. Mookherjee, L. Stixrude, *Phys. Chem. Miner.* **37**, 103 (2010).
27. E. M. Stolper, *Geochim. Cosmochim. Acta* **46**, 2609 (1982).
28. L. Stixrude, N. de Koker, N. Sun, M. Mookherjee, B. B. Karki, *Earth Planet. Sci. Lett.* **278**, 226 (2009).
29. The Rayleigh and Prandtl numbers are $\mathrm{Ra} = [\alpha\rho g(T_M - T_S)L^3]/(\kappa\eta)$ and $\mathrm{Pr} = \eta/(\rho\kappa)$. We have adopted the density (ρ = 4410 kg m^{-3}) and thermal expansivity ($\alpha = 2.6 \times 10^{-5}$) (*16*) and assumed the depth scale L = 3000 km, acceleration due to gravity g = 10 m s^{-2}, thermal conductivity k = 1.2 W m^{-1} K^{-1} (*33*), thermal diffusivity $\kappa = k/(\rho c_P)$ where the specific heat c_P = 1660 J kg^{-1} K^{-1} (*16*), a mantle potential temperature T_M = 2500 K, the lowest temperature at which the mantle will be completely molten, and a surface temperature T_S = 1000 K set by a dense atmosphere (*2*).
30. The surface heat flux is $F = 0.22k(T_M - T_S)\mathrm{Ra}^{2/7}\mathrm{Pr}^{-1/7}L^{-1}$ (*34*) and the cooling time is $\tau_{cool} = T_M c_P M_M/4\pi R^2 F$, where M_M is the mass of the mantle and R is the radius of Earth.
31. S. Labrosse, J. W. Hernlund, N. Coltice, *Nature* **450**, 866 (2007).
32. G. Kresse, J. Furthmuller, *Comput. Mater. Sci.* **6**, 15 (1996).
33. A. M. Hofmeister, A. G. Whittington, M. Pertermann, *Contrib. Mineral. Petrol.* **158**, 381 (2009).
34. B. I. Shraiman, E. D. Siggia, *Phys. Rev. A* **42**, 3650 (1990).
35. K. R. Harris, L. A. Woolf, M. Kanakubo, *J. Chem. Eng. Data* **50**, 1777 (2005).

36. This work was supported by NSF (EAR-0809489) and the UK National Environmental Research Council (NE/F01787/1). Computing facilities were provided by the Center of Computation and Technology at Louisiana State University. The authors thank J. Brodholt, M. Ghiorso, and S. Karato for useful comments and suggestions.

Supporting Online Material

www.sciencemag.org/cgi/content/full/328/5979/740/DC1
Materials and Methods
Figs. S1 and S2

16 February 2010; accepted 7 April 2010
10.1126/science.1188327

Extreme Deuterium Excesses in Ultracarbonaceous Micrometeorites from Central Antarctic Snow

J. Duprat,[1]* E. Dobrică,[1] C. Engrand,[1] J. Aléon,[1] Y. Marrocchi,[2] S. Mostefaoui,[2] A. Meibom,[2] H. Leroux,[3] J.-N. Rouzaud,[4] M. Gounelle,[2] F. Robert[2]

Primitive interplanetary dust is expected to contain the earliest solar system components, including minerals and organic matter. We have recovered, from central Antarctic snow, ultracarbonaceous micrometeorites whose organic matter contains extreme deuterium (D) excesses (10 to 30 times terrestrial values), extending over hundreds of square micrometers. We identified crystalline minerals embedded in the micrometeorite organic matter, which suggests that this organic matter reservoir could have formed within the solar system itself rather than having direct interstellar heritage. The high D/H ratios, the high organic matter content, and the associated minerals favor an origin from the cold regions of the protoplanetary disk. The masses of the particles range from a few tenths of a microgram to a few micrograms, exceeding by more than an order of magnitude those of the dust fragments from comet 81P/Wild 2 returned by the Stardust mission.

The light element isotopic compositions of undifferentiated interplanetary material provide insights into the physicochemical processes that took place in the coldest regions of the early solar system. Large deuterium excesses are expected in the solid component(s) of comets because their water and HCN molecules exhibit D/H ratios from 2 to 15 times the terrestrial value, respectively (*1*). However, isotopic measurements of fragments of comet 81P/Wild 2 returned by the Stardust mission show moderate D/H ratios that do not exceed three times the terrestrial value, possibly indicating a substantial alteration during impact capture process (*2*). By contrast, large D/H ratios have been observed as micrometer-sized hot spots in organic matter of interplanetary dust particles (IDPs) (*3*, *4*) or primitive meteorites (*5*, *6*). These D excesses may have been inherited from the cold molecular cloud that predated the protosolar nebula (*3*, *5*, *7*) or may be the result of a local process that occurred in the cold outer regions of the protoplanetary disk (*8*, *9*). The nature of the D-rich hot spots and their relationship to the organic matter bulk composition remain a matter of debate (*6*, *10*). Organic matter in meteorites is sparse and disseminated in the matrix, with a maximum bulk concentration on the order of a few weight percent (wt %) (*11*). It is mainly accessible as the acid-insoluble component (IOM) remaining after demineralization of large amounts (grams) of primitive meteorites.

Large numbers of Antarctic micrometeorites (AMMs), which are IDPs with sizes ranging from 20 to 1000 μm, can be recovered from the Antarctic ice cap (*12*). Here, we describe AMMs obtained from the melting and sieving of 3 m^3 of ultraclean snow that fell in the vicinity of the French-Italian CONCORDIA station at Dome C

[1]Centre de Spectrométrie Nucléaire et de Spectrométrie de Masse, Université Paris-Sud 11, CNRS/IN2P3, F-91405 Orsay, France. [2]Laboratoire de Minéralogie et Cosmochimie du Muséum (LMCM), UMR 7202–CNRS INSU, Muséum National d'Histoire Naturelle, 57 Rue Cuvier, 75231 Paris Cedex 05, France. [3]Unité Matériaux et Transformations, Université Lille 1 & CNRS, 59655 Villeneuve d'Ascq, France. [4]Laboratoire de Géologie de l'Ecole Normale Supérieure, UMR CNRS 8538, 24 rue Lhomond, 75231 Paris Cedex 5, France.

*To whom correspondence should be addressed. E-mail: jean.duprat@csnsm.in2p3.fr